Flow structures with high Lagrangian coherence promote diatom blooms in oligotrophic waters

Ismael Hernández-Carrasco[1], Vincent Rossi[2], Gabriel Navarro[3], Antonio Turiel[4], Annalisa Bracco[5], Alejandro Orfila[1]

[1]Mediterranean Institute for Advanced Studies (UIB-CSIC), Miquel Marqués, 21. E-07190 Esporles, Spain
[2]Mediterranean Institute of Oceanography, CNRS UMR 7294, Campus de Luminy, 13288 Marseille, France
[3]ICMAN (CSIC), Campus Rio San Pedro. E-11519. Puerto Real. Cadiz, Spain
[4]ICM (CSIC), Passeig Marítim de la Barceloneta, 37-49. E-08003 Barcelona, Spain
[5]School of Earth and Atmospheric Sciences, Georgia Institute of Technology, Atlanta, 30306, Georgia, USA

Key Points:

- We provide an objective measure of the range of dynamical coherence scales in geophysical flows
- We propose the Lagrangian coherence scale as a new metric to classify biologically relevant flow structures
- Observations evidence that turbulent flow structures with a high Lagrangian coherence are conductive to diatom blooms in oligotrophic waters.

Corresponding author: Ismael Hernández-Carrasco, ihernandez@imedea.uib-csic.es

Abstract

Diatoms are among the most efficient marine organisms for primary production and carbon sequestration, absorbing at least 10 billion tonnes of carbon dioxide every year. Yet, the spatial distributions of these planktonic organisms remain puzzling and the underlying physical processes poorly known. Here we investigate what dynamical conditions are conductive to episodic diatom blooms in oligotrophic waters based on Lagrangian diagnosis and satellite-derived phytoplankton functional types and ocean currents. The Lagrangian coherence of the flow is diagnosed in space and time simultaneously to identify which structures favor diatom growth. Observations evidence that flow structures with a high degree of coherence (40 days or longer) in high turbulent kinetic energy and vorticity sustain high concentrations of diatoms in the sunlite layers. Our findings show that the integration of Eulerian kinematic variables into a Lagrangian frame allows revealing new dynamical aspects of geophysical turbulence and unveil transport properties having large biological impacts.

Plain Language Summary

Marine diatoms is a photosynthetic plankton group that plays an important role in the generation of oxygen and the removal of carbon dioxide from the atmosphere. However, their abundance is predicted to decline as a result of the increasing ocean stratification induced by global warming. Understanding the underlying physical processes that are conductive to diatom blooms is crucial to accurately predict the evolution of primary production and carbon export. Here using an objective measure of the range of dynamical coherence scales and satellite observations, we provide evidences that flow structures with a high degree of coherence in high turbulent kinetic energy and vorticity track the favorable dynamical conditions sustaining diatoms growth in stratified and oligotrophic waters.

1 Introduction

Earth System model simulations as well as mesocosm experiments indicate that in response to increased ocean stratification and reduced vertical mixing caused by global warming, diatoms are likely to decline or be replaced by smaller phytoplankton (Barton et al., 2016; Frémont et al., 2022). However, these model predictions do not account for the role of the physical environment at scales smaller than 100 km in structuring the distribution of phytoplankton functional types. Understanding the role played by the ocean circulation at these scales in the development of diatoms in stratified and oligotrophic waters is essential to accurately predict the future evolution of primary production and carbon export (Falkowski et al., 1998; Field et al., 1998; Tréguer et al., 2018).

In contrast to other groups of smaller plankton, such as dinoflagellates, which are favored under stratified (low-turbulent), low-nutrient conditions (Glibert, 2016), diatoms are known to thrive in high nutrient-high turbulent systems (e.g. polar, upwelling and coastal areas). They are, however, not exclusive to these systems, and recent observations revealed that short-living spatially-restricted diatoms blooms may occur in oligotrophic, nutrient limited waters (Malviya et al., 2016), fueled by transient meso- and submesoscale dynamical structures such as eddies, fronts or filaments (Tréguer et al., 2018; Hernández-Carrasco et al., 2020). However it is not yet possible to link specific dynamical structures to functional phytoplankton groups. On one hand, model-based studies are strongly dependent on the modeling formulation and how the interactions between biological and physical processes are parameterized (Barton et al., 2010; D. J. McGillicuddy, 2016). Observational studies, on the other hand, remain scarce due to the lack of simultaneous measurements of velocity fields and phytoplankton taxonomy at synoptic scale (Hernández-Carrasco et al., 2020). Furthermore, most monitoring studies occur at a fixed location, linking the characteristics of the local phytoplankton communities to some prop-

erties of the Eulerian ("frozen" in space) flow (Cotti-Rausch et al., 2016). Contrasting with the Eulerian view, an important issue when studying bio-physical interactions in fluid environments is that any physically-driven phytoplankton community shift or change in activity (Lévy et al., 2014; Wilkins et al., 2013) would reflect the cumulative effects of coherent transport dynamics affecting nutrient supply and other growth limiting factors.

In this study we propose a methodology to classify the flow structures according to their Lagrangian coherence scales. The method is based on the Lagrangian assessment F of Eulerian kinematic variables f, which provides information on the cumulative effect of f along trajectories, as it integrates the observed variable over the time-evolution of moving water parcels arriving to a specific point. The finite-time dynamical systems theory has shown that relevant information regarding the dynamical properties of the flow can be inferred from F, especially when f is chosen to be a function related to the velocity field (Haller & Poje, 1998; Mezić et al., 2010). We assess coherent transport processes through the finite-time Lagrangian integration of vorticity and eddy kinetic energy (EKE), denoted by Ω_T and K_T, respectively. The proposed methodology allows for investigating the impact of Lagrangian persistent lateral turbulent properties of the underlying flow structures on the phytoplankton community structure. In particular, we can accurately assess the spatial and temporal coherence scales of turbulent structures that do or do not favor a sustained growth of diatoms, providing a robust diagnostic to identify, among all the eddies, those associated with a biological response. Previously developed Lagrangian flow diagnostics, such as Lyapunov exponents based Lagrangian coherent structures (Hernández-Carrasco et al., 2011) have shown to be very useful to identify dynamical boundaries separating different functional phytoplankton groups (d'Ovidio et al., 2010). However, the proposed methodology allows further identifying not only the boundaries but also the dynamical characteristic scales of the underlying flow associated with a particular functional phytoplankton group. We apply this framework to data from two independent sources of satellite observations. Specifically, we use data of dominant phytoplankton functional type (PFT) from a regional adaptation of the PHYSAT algorithm (Navarro et al., 2017) and daily velocity fields at $1/8^\circ$ of spatial resolution derived from a Ssalto/Duacs multimission altimeter regional product.

We focus on the Mediterranean Sea, which is characterized by intense mesoscale activity (d'Ovidio et al., 2009; Morales-Márquez et al., 2022) and by high productivity only during spring time, between February and April (Basterretxea et al., 2018), with dominance of large phytoplanktonic cells such as diatoms (Navarro et al., 2017). During the rest of the year is on average oligotrophic and highly stratified, disrupted by local - in time and space - events of elevated phytoplankton growth. The Mediterranean Sea is therefore a good proxy for ocean deserts, which cover most of the global ocean, offering an ideal laboratory to explore the biological response of an oligotrophic and highly stratified environment to intermittent, dynamical changes in the physical structure of the upper ocean.

2 Finite-time Lagrangian diagnostics

Given a Eulerian descriptor f, its Lagrangian counterpart F can be obtained by computing the path-integral of f. They can be expressed in a general way by the material integration of f along the fluid parcel trajectory, $\mathbf{R}_T(\mathbf{r}_0, t_0)$, initially located at $\mathbf{r}_0(t_0)$ over a finite time interval of integration T as, $F_T(\mathbf{r}_0, t_0) = \frac{1}{T}\int_{t_0}^{t_0+T} f(\mathbf{R}_t(\mathbf{r}, t_0), t)dt$. The ergodic theory of dynamical systems asserts that when $\mathrm{T} \to \infty$ such Lagrangian functions should be constant along invariant manifolds, independently of the Eulerian function chosen. This property has been used to extract the flow geometry in autonomous or periodic dynamical systems (Haller & Poje, 1998). Nevertheless the ocean flow is dynamically an aperiodic and finite system; consequently such functions can only be path-integrated (or averaged in a Lagrangian sense) over a finite time period ($\mathrm{T} << \infty$). Even

so, relevant information regarding the dynamical properties of the flow can still be inferred from F, especially when f is chosen to be a function related to the velocity field, $\mathbf{v}$ (Haller & Poje, 1998; Mezić et al., 2010). Here we quantify transport coherent processes extending the choice of these functions to relative vorticity (ω) and eddy kinetic energy (EKE), since EKE informs on the turbulent component of the flow associated with eddy activity, while ω takes into account the shear and the rotation of the flow.

The Lagrangian description of the vorticity was originally reported in Casey, 1991 (Casey & Naghdi, 1991) and recently used to develop an objective identification of coherent vortex boundaries based on well-defined contours of Lagrangian-averaged vorticity deviation (LAVD) (Haller et al., 2016). Considering the motion of a fluid parcel on the time interval [t_0, t_0+T] in an incompressible two dimensional flow, we define the finite-time Lagrangian vorticity (FTLV), denoted by Ω_T, at the position $\mathbf{r}_0 = (x_0, y_0)$ at time t_0 as,

$$\Omega_T(\mathbf{r}_0, t_0) = \frac{1}{T}\int_{t_0}^{t_0+T} \omega(\mathbf{R}_t(\mathbf{r}, t_0), t)\, dt, \tag{1}$$

where ω is the Eulerian relative vorticity: $\omega(\mathbf{r}, t) = \frac{\partial v(\mathbf{r},t)}{\partial x} - \frac{\partial u(\mathbf{r},t)}{\partial y}$.

Furthermore we introduce a new metric to analyze the evolution of the EKE along fluid parcel trajectories. Specifically, we compute the finite-time Lagrangian EKE (FTLK), denoted by K_T, as follows,

$$K_T(\mathbf{r}_0, t_0) = \frac{1}{T}\int_{t_0}^{t_0+T} \kappa(\mathbf{R}_t(\mathbf{r}, t_0), t)dt, \tag{2}$$

where κ is the Eulerian EKE given by, $\kappa(\mathbf{r}, t) = (u(\mathbf{r}, t) - \langle u(\mathbf{r})\rangle_{\Delta T})^2 + (v(\mathbf{r}, t) - \langle v(\mathbf{r})\rangle_{\Delta T})^2$, obtained through the instantaneous anomaly of the zonal and meridional components of the velocity field with respect to the steady mean of the total kinetic energy, which is achieved averaging over a time period of ΔT=10 years. This diagnostic allows classifying the flow, in the domain under consideration, in subregions according to the Lagrangian-persistent level of the turbulent mesoscale activity. High values of K_T identify therefore regions where the flow is concentrating turbulent energy. The selection of the time integration, T, depends on the typical time scales of the process to be studied.

3 Satellite data

The identification from satellite observations of the dominant phytoplankton functional type (PFT), is performed using the PHYSAT algorithm (Alvain et al., 2005). Here we use a regional adaptation of this algorithm to the specific bio-optical characteristics of the Mediterranean Sea, PHYSAT-Med (Navarro et al., 2014, 2017). The PHYSAT-Med identifies nanoeukaryotes, coccolithophorids, *Prochlorococcus*, *Synechococcus*-like cyanobacteria, diatoms and Phaeocystis-like phytoplankton through the analysis of the specific signatures in the normalized water leaving radiance (nLw) spectra measured by ocean color sensors. For this study, we use the PHYSAT-Med version published in 2017 (Navarro et al., 2017), in which the authors used the OC-CCI v3.0 dataset generated from merged normalized remote-sensing reflectance derived from four satellite sensors (Storm et al., 2013): SeaWiFS, MODIS, MERIS, and VIIRS. PHYSAT-Med retrieves the dominant group for a given satellite image pixel (4 km for the Mediterranean Sea) by identifying which phytoplankton group is the major contributor to the radiance anomaly. In other words, it associates a given phytoplankton type with its main bio-optical signature, while taking into account biases induced by other optically-active components, such as dust deposition events and rivers discharge. From this high-resolution database (about 6,600 daily images), 10-day and monthly maps of dominant phytoplankton groups were obtained by calculating the phytoplankton group that was dominant during the integration period (10-day or monthly, respectively) at each geographical pixel, not including "unidentified" pixels. The regional PHYSAT-Med product was validated by comparing

the outputs of the algorithm with more than 5,000 in situ measurements analyzed by high-performance liquid chromatography (HPLC) (Navarro et al., 2014, 2017).

The current flow field is derived from daily absolute geostrophic surface velocities at 1/8° of spatial resolution derived from a Ssalto/Duacs multimission altimeter regional product released in 2016 specific for the Mediterranean Sea. This product is currently distributed by the Copernicus Marine Environment Monitoring Service (CMEMS).

4 Results

Dynamical co-coherence of oceanic flow features

We first discuss how the flow characterization inferred from a given kinematic quantity differs when evaluated through either Eulerian or Lagrangian functions. The latter are not directly related to instantaneous measurements of such functions, unless some kind of dynamic equilibrium or ergodicity-type property is established. In this case, the time-integrated effect can be effectively related to the instantaneous or averaged spatial patterns (for instance, if the spatial arrangement of eddies at a given time provides information about the typical time evolution of a water parcel). Using daily gridded geostrophic velocities derived from altimetry (see section 3) we compare daily snapshots of the Eulerian vorticity and EKE, denoted by Ω_0 and K_0, respectively, (Fig. 1*A* and 1*C*), and their Lagrangian counterpart evaluated for T=40 days, Ω_{40} and K_{40} (Fig. 1*B* and 1*D*) (see Section 2 for a detailed description of these metrics). Spatial patterns of Ω_T and K_T differ significantly from their Eulerian equivalence whenever the integration time is greater than 15 days (see Fig. S1 in the Supporting Information). Filamentary structures of intense accumulated vorticity and EKE around and within the eddies that could originate from eddy-flow or eddy-eddy interactions are unveiled by the Lagrangian diagnostic but not by the Eulerian one. Furthermore, some structures with high values of vorticity and EKE identified by Ω_0 and K_0 vanish in Ω_{40} and K_{40}, suggesting that these structures are not dynamically persistent, while only the highly coherent flow structures remain as T increases (Fig. S2 in the Supporting Information). The above analysis suggests that the Lagrangian characterization of the marine turbulent flow unveils super-coherent structures, i.e singular structures of high dynamical coherence, that can not be identified in the classical Eulerian framework.

To assess how the Ω_T and K_T scale with the duration of integration, we analyze their statistical behavior comparing the probability density functions (PDF) of Ω_T and K_T for different T values (Fig. 1*E* and 1*F*). As T increases the peak of the PDFs increases while their width narrows, and the PDF becomes asymmetrical, with a more pronounced tail for negative vorticity values and high EKE values. This PDF behaviour - a time-dependent histogram whose peak becomes sharper and higher as the time integration lengthens - is characteristic of a multifractal scaling (Falconer, 1990; Hernández-Carrasco et al., 2011), often used to interpret spatial scales but extended here to temporal scales.

Given that in the ocean nearly 80% of the total kinetic energy is captured in vortical coherent structures (Klein et al., 2019), a relationship between Eulerian EKE and vorticity may be expected. However when comparing the spatial patterns of both Eulerian quantities (Fig. 1*A*, *C*), we do not find a clear correspondence. Conversely, the spatial distribution is very similar when comparing their Lagrangian counterparts (Fig. 1*B*, *D*). To further study the relationship between Ω_T and K_T we examine the histograms of Ω_T conditioned by the value of K_T for different values of T (Fig. 2). It allows exploring which aspects of the flow dynamical coherence is well-captured by the Lagrangian assessment but missed by the Eulerian approach. We observe a dispersed cloud of points for T=0 days (Fig. 2*A*), while a clear modal line (e.g. line of maximum conditioned probabilities) formed by two different, nearly straight, segments is evident for T=40 days (Fig.

$2B$). These segments are associated with a slowly increasing and faster decreasing dependency of Ω_T with K_T, respectively. In order to verify if a functional dependence between vorticity and EKE could hold for our dataset, we compute various conditioned averages $\hat{\Omega}_T(K_T)$ for different integration times T (Fig. $2C$). While the plot shows conditioned averages, the conditioned standard deviation is not negligible as reflected by the correlation coefficients R^2 and associated slopes reported in the caption of Fig. 2. While there is a very weak relationship among Eulerian quantities (black curve), we observe more robust relationships as T increases (green curves). The resulting conditional mean is a constant value for K_T smaller than 0.13 m^2/s^2 suggesting that Ω_T and K_T are statistically independent, and there is not a functional relationship between the two variables at low values of EKE. A functional relationship, on the other hand, exists for values of K_T greater than 0.13 m^2/s^2. Overall, Fig. $2C$ suggests that we can approximate Ω_T in terms of $(K_T)^{1/2}$ allowing to infer a spatial scale, L, from the slopes A after fitting: $\Omega_T = A \cdot (K_T)^{1/2}$ ($L = 1/A$) for high values of $(K_T)^{1/2}$. L has units of the inverse of length (1/m) and provides an estimation of the spatial scale associated with the coherence of these Lagrangian structures and their evolution as a function of the time integration. It could be interpreted as the typical length-scales of the vortical structures that contribute most, and for longer times, to the turbulent energy. Values of L decreases as T increases, with values ranging between [60 - 15 km] for T = [0 - 80 days], indicating that when T increases smaller structures are captured. The minimum L value in the flow considered converges to 15 km, which represents the smallest length-scale of the Lagrangian dynamical structures that can be inferred from this velocity field.

The high correlation between Ω_T and K_T for T > 40 days, indicates that spatial variations of Lagrangian coherent vorticity are closely related to spatial variations of Lagrangian coherent mesoscale activity. This suggests that the persistent anticyclonic eddies in the portion of Mediterranean Sea analyzed emanate fluid parcels associated with accumulated mesoscale turbulent energy. Consequently, Ω_T for T > 40 days is a more suitable Lagrangian diagnostic to link turbulence properties to phytoplankton dynamics than its Eulerian counterpart (T = 0 days), whenever the analyzed flow is derived from altimetry.

Influence of oceanic coherence on the phytoplankton community composition

Here we dive on the response of diatoms to the ocean physical conditions focusing on the Lagrangian coherence scales of the marine flow structures unveiled by these novel metrics. Figure $3A$ shows a patchy spatial distribution of chlorophyll-a concentration, a proxy of total phytoplankton, with local maxima dominated by diatoms (Fig. $3B$), located at 38.5°N/5.5°E. In order to compare with PHYSAT-Med images, which correspond to a 10 days averaged distribution of phytoplankton types, we show the spatial patterns of time averaged snapshots of Eulerian vorticity, Ω_0,and EKE, K_0, over the same 10 days in Fig. $3C$ and Fig. $3E$, revealing different structures of high vorticity and EKE distributed throughout the entire area. This map is significantly different from the time average over the same 10 days of daily snapshots of Lagrangian vorticity (Ω_{40}, Fig. $3D$) and Lagrangian EKE (K_{40}, Fig. $3F$) for T=40 days. Only one intense eddy-like structure stands out among all other structures inferred from Ω_0 and K_0. It indicates again that while Eulerian flow structures assess coherence in the spatial domain, Lagrangian structures can assess coherence in space and time simultaneously. As such, most-eddy like structures identified by Ω_0 and K_0 and vanishing in the Ω_T and K_T fields for T > 40 days exhibit spatial coherence only; conversely, the central eddy is unique exhibiting high coherence over both space and time. By combining both Lagrangian metrics we can identify singular supercoherent vortical objects associated with high mesoscale turbulent energy which should impact plankton communities.

Comparing the maps of Ω_0 and K_0 (Fig. 3*C* and *E*, respectively) with the spatial distribution of the dominant phytoplankton groups (Fig. 3*B*) we observe that the confined and circular patch dominated by diatoms is associated with local maxima of EKE and extrema (both positive and negative) of vorticity. However, the reciprocal statement is not true: not all local maxima of both Eulerian quantities are characterized by diatoms. Looking at the Ω_T and K_T diagnostics (Fig. 3*D* and *F*), we found the singular structure associated with high Lagrangian turbulent kinetic energy and vorticity values uniquely identifies the diatoms bloom. In the Eulerian framework, many structures of high EKE and vorticity are present in the domain without a clear correspondence with any dominant phytoplankton group. Conversely, our novel Lagrangian diagnostics distinguish singular coherent structures that support specific biological response from the other transient features that have no clear biological signal. Further examples of the correspondence between these coherent dynamical objects and diatom blooms are shown in Supporting Information (Fig. S3 to S11).

The co-occurrence between diatoms blooms and these singular dynamical structures suggests a relationship between the abundance of diatoms and the degree of coherence of the oceanic features. To further explore this relationship we compute the probability density functions of the diatom abundances, henceforth referred to as P(diatoms), conditioned by different discretized values of Ω_T and K_T (50 bins are taken) and for different values of T averaged over 15 diatom blooms x 30 snapshots/event distributed in the stratification period (May-September) among the analyzed 10 years of PHYSAT-Med data. Area-normalized PDFs (Fig. 4*A* and *B*) have a characteristic signature that becomes flatter at lower values of Ω_T and K_T as the time integration lengthens. When T = 0 higher values of P(diatoms) are found in regions characterized by low values of vorticity and turbulence, and high P(diatoms) values shift toward higher values of vorticity and turbulent kinetic energy as T increases. The drifting fluid parcels that largely contribute to promoting diatom growth are those that preserve high negative vorticity and turbulent kinetic energy while they move with the flow for a sufficiently long amount of time. The shape of the histograms persists nearly unaltered from T = 40 to T = 80 days. While the existence of this 'collapsed' shape of the histogram confirms the need to use a Lagrangian approach to identify the flow properties that matters for biological variables, it further suggests that 40-80 days is the characteristic time-scale of bio-physical interactions most relevant to predict/explain localized diatom blooms.

In order to estimate the optimal time scale of the flow coherence that maximizes bio-physical interactions, we compute the area-normalized number of pixels where diatoms dominate (i.e. the number of pixels identified as diatoms normalized by the total area of high Ω_T and high K_T, that is a proxy of diatoms relative abundance) over regions characterized by high values of Ω_T and K_T fields (defined as $\Omega_T/\mathrm{f} > 0.1$ or $<$ -0.1 for negative vorticity and $K_T > 0.1$ m^2/s^2) as a function of T. The abundance of diatoms increases in regions of high negative Lagrangian vorticity (Fig. 4*C*) while decreases in regions of positive Lagrangian vorticity as T increases (Fig. 4*E*). This asymmetric behavior is opposite to that recovered through Eulerian analyses (Ω_0) in which diatoms appear associated predominantly with coherent (in space only) positive vorticity. This counter-intuitive behavior is explained by the fact that fluid parcels with positive/negative vorticity at time t_0 may have had opposite sign vorticity when the whole history of the parcel is considered (i.e integrating the relative vorticity backward in time from t_0 to t_0 - T $>$ 0 days). For example fluid parcels coming from an anticyclonic/cyclonic eddy can be absorbed by an cyclonic/anticyclonic eddy (Hernández-Carrasco et al., 2020). For both high negative and positive Ω_T we observe a plateau in P(diatoms) for T$>$ 70 days. A similar behavior is identified when looking at P(diatoms) in regions of high Lagrangian turbulent kinetic energy ($K_T > 0.1$ m^2/s^2) for different T. The probability to find high abundance of diatoms increases with T and reaches its maximum value for T = 30 days (Fig. 4*D*). By simultaneously conditioning the abundance of diatoms in regions of high Ω_T (either positive or negative) together with K_T (Fig. 4*F*), we find that P(diatoms) associated with these turbulent flow conditions initially increases over in-

tegration time and reaches a plateau for T > 40 days. From this T threshold, one can infer the optimal coherence time of vortical structures for diatoms blooms under stratified, oligotrophic conditions.

5 Discussion and conclusions

To understand the effects of global warming on global ocean physical and biogeochemical properties, it is essential to identify the scales that are relevant for dynamical and biological interactions, and then predict their evolution. The coherence analysis of the surface ocean dynamics through the Lagrangian descriptors, K_T and Ω_T provides for the first time a theoretically-grounded and objective measure of the range of dynamical coherence time and spatial scales associated with mesoscale ocean features. We show that the relationship between EKE (K_T) and vorticity (Ω_T) emerges for topological structures characterized with high dynamical coherence. As T increases the Lagrangian vorticity and the EKE field emerge organized in filaments of high values. In the case of the altimetry velocity field analyzed here, we find a dynamical resolution barrier with Lagrangian flow structures size converging and collapsing at spatial scale L=[15-20 km] for time scales of coherence T > 40 days. At these scales the filamentary dynamics associated with the fine-mesoscale turbulence becomes relevant. This is likely due to the vortex filaments induced by the (mesoscale) eddy-eddy interactions and their contribution to the energy cascade from large to small scales (in nature down to the submesoscales, which are not well captured by current altimetry, but will be partially resolved by the future SWOT mission (Morrow et al., 2019)). This Lagrangian similarity between different kinematic flow properties can be used to assess the finest effective scales of the dynamics captured in a given velocity field, as well as to evaluate the capability of models or observations to resolve different processes.

The Lagrangian description of vorticity and turbulent energy through K_T and Ω_T does offer some advantages as shown by comparing it with the conventional (Eulerian) description. The Lagrangian objects uniquely identified as high-coherent turbulent eddies track the favorable dynamical conditions, namely a turbulent environment that is sufficiently coherent in space and time, favouring diatoms growth. This allows to differentiate the mesoscale structures that effectively promote diatoms blooms from those that only stir existing communities (d'Ovidio et al., 2010). Analyzing the accumulated effect of the flow dynamical properties along fluid parcel trajectories hosting phytoplankton cells allows for estimating the typical time and length scales at which the interactions between the dynamical flow and the fast-growing opportunist planktonic groups (diatom-like in our case) are most significant. We observe that T = 40 days is a critical coherence time scale at which the mesoscale turbulent conditions (i.e. vorticity and EKE) influence phytoplankton community composition by promoting diatoms, through persistent cell re-suspension and nutrient vertical fluxes favoring their encounter in the euphotic zone. This value is of the same order of magnitude but slightly smaller than the 60 days of mean life associated with non-linear eddies that display the maximum correlation with high concentrations of surface Chl *a* reported in previous studies (Chelton et al., 2011).

The limited resolution of the altimetry currents implies that we cannot quantify the biological response of rapidly fluctuating small scale structures but only the slow dynamics, i.e. temporal scales longer than 1 week. It should be noted that using a coarse velocity field (coarser than in the real ocean) may introduce spurious Lagrangian dynamics at small scales (Haza et al., 2016), but does not impact the dynamics at scales larger than resolution, that remains robust (Beron-Vera et al., 2019; Hernández-Carrasco et al., 2011). This ensures that the resolution in the altimetry dynamical fields is not affecting the evaluation of the temporal scales at or above 40 days at which diatoms 'feel' the flow coherence. This is evident in Fig. 4C, where the concentration of diatoms in structures of high vorticity increases as a a function of Lagrangian integration up to T=70 days, which is longer than the critical scale of 40 days identified by the Lagrangian ef-

fective resolution analysis. Our findings, based on satellite observations, provide a robust target against which models can be now tested to verify their ability to properly represent physical-biogeochemical interactions. Mesoscale resolving regional simulations should indeed capture the diatom preferences, at the relevant spatial and temporal coherence scales, that we identified. In interpreting our results, we excluded the possibility that the fluid parcels with high diatom concentrations are composed of nutrient rich coastal waters by analyzing the origin maps shown in the Supporting Information (Fig. S12-S14). This suggests that diatom growth occurs whenever diatoms in resting stages, likely present at low concentrations in most of the surface ocean (Rynearson et al., 2013) (even oligotrophic), are entrained in coherent physical structures and can exploit vertical mixing events (e.g. ephemeral hot spots of intense vertical fluxes (D. McGillicuddy et al., 1998; Falkowski et al., 1998; Klein & Lapeyre, 2009; Lévy et al., 2018)) induced by specific mesoscale eddies that persist for enough time (more than one month). Indeed, our analysis allows for identifying these short-living and moving diatoms habitats despite high-stratification conditions typical of "oceanic deserts", as the major oligotrophic gyres of the world ocean.

6 Open Research

Absolute geostrophic velocity data are available on the CMEMS web platform `https://data.marine.copernicus.eu/products` and at `DOI:10.48670/moi-00141`. PHYSAT-Med data are referenced at Navarro et al., 2017 and are available at `https://nimbus.imedea.uib-csic.es/index.php/s/6w6YzWBpTmWD8BW`. The code to compute the particle trajectories and the Finite-Time Lagrangian diagnostics are available at `https://doi.org/10.5281/zenodo.7705122` with Creative Commons Attribution 4.0 International licence. Figures are plotted using Matlab v2021 software.

Acknowledgments

IH-C acknowledges financial support from the project TRITOP (grant# UIB2021-PD06) funded by University of the Balearic Islands and by FEDER(EU). AO thanks financial support from Projects LAMARCA (PID2021-123352OB-C31) funded by MICIN/AEI /10.13039/501100011033/ FEDER, UE and Tech2Coast (TED2021-130949B-I00) funded by MCIN/AEI/ 10.13039/501100011033 and BY EU 'NextGenerationEU/PRTR'. AB acknowledges support from the National Science Foundation (grant OCE-1658174). This study is based upon work from the CSIC Interdisciplinary Thematic Platform (PTI) Teledeteccion (PTI-TELEDETECT) members

References

Alvain, S., Moulin, C., Dandonneau, Y., & Bréon, F. (2005). Remote sensing of phytoplankton groups in case 1 waters from global SeaWiFS imagery. *Deep Sea Research Part I: Oceanographic Research Papers*, *52*(11), 1989 - 2004. doi: https://doi.org/10.1016/j.dsr.2005.06.015

Barton, A. D., Dutkiewicz, S., Flierl, G., Bragg, J., & Follows, M. J. (2010). Patterns of diversity in marine phytoplankton. , *327*(5972), 1509–1511. doi: 10.1126/science.1184961

Barton, A. D., Irwin, A. J., Finkel, Z. V., & Stock, C. A. (2016). Anthropogenic climate change drives shift and shuffle in North Atlantic phytoplankton communities. *Proceedings of the National Academy of Sciences*, *113*(11), 2964-2969. doi: 10.1073/pnas.1519080113

Basterretxea, G., Font-Muñoz, J. S., Salgado-Hernanz, P., Arrieta, J., & Hernández-Carrasco, I. (2018). Patterns of chlorophyll interannual variability in Mediterranean biogeographical regions. *Remote Sensing of Environment*, *215*, 7 - 17. doi: 10.1016/j.rse.2018.05.027

Beron-Vera, F. J., Hadjighasem, A., Xia, Q., Olascoaga, M. J., & Haller, G.

(2019). Coherent lagrangian swirls among submesoscale motions. *Proceedings of the National Academy of Science*, *116*(37), 18251-18256. doi: 10.1073/pnas.1701392115

Casey, J., & Naghdi, P. M. (1991). On the lagrangian description of vorticity. *Archive for Rational Mechanics and Analysis*, *115*(1), 1–14. doi: 10.1007/BF01881677

Chelton, D., Gaube, P., Schlax, M., Early, J., & Samelson, R. (2011). The influence of Nonlinear Mesoscale Eddies on Near-Surface Oceanic Chlorophyll. *Science*, *334*, 328–332. doi: 10.1126/science.1208897

Cotti-Rausch, B. E., Lomas, M. W., Lachenmyer, E. M., Goldman, E. A., Bell, D. W., Goldberg, S. R., & Richardson, T. L. (2016). Mesoscale and submesoscale variability in phytoplankton community composition in the Sargasso Sea. *Deep Sea Research Part I: Oceanographic Research Papers*, *110*, 106-122. doi: https://doi.org/10.1016/j.dsr.2015.11.008

d'Ovidio, F., Isern-Fontanet, J., López, C., Hernández-García, E., & García-Ladona, E. (2009). Comparison between Eulerian diagnostics and Finite-Size Lyapunov Exponents computed from altimetry in the Algerian basin. *Deep-Sea Res. I*, *56*, 15–31. doi: 10.1016/j.dsr.2008.07.014

d'Ovidio, F., Monte, S., Alvain, S., Dandonneau, Y., & Levy, M. (2010). Fluid dynamical niches of phytoplankton types. *Proc. Natl. Acad. Sci.*, *107*, 18366. doi: 10.1073/pnas.1004620107

Falconer, K. (1990). *Fractal geometry: Mathematical foundations and applications.* Chichester: John Wiley and sons.

Falkowski, P. G., Barber, R. T., & Smetacek, V. (1998). Biogeochemical Controls and Feedbacks on Ocean Primary Production. *Science*, *281*(5374), 200–206. doi: 10.1126/science.281.5374.200

Field, C. B., Behrenfeld, M. J., Randerson, J. T., & Falkowski, P. (1998). Primary production of the biosphere: Integrating terrestrial and oceanic components. *Science*, *281*(5374), 237–240. doi: 10.1126/science.281.5374.237

Frémont, P., Gehlen, M., Vrac, M., Leconte, J., Delmont, T. O., Wincker, P., ... Jaillon, O. (2022). Restructuring of plankton genomic biogeography in the surface ocean under climate change. *Nature Climate Change*, *12*, 393-401. doi: 10.1038/s41558-022-01314-8

Glibert, P. M. (2016). Margalef revisited: A new phytoplankton mandala incorporating twelve dimensions, including nutritional physiology. *Harmful Algae*, *55*, 25 - 30. doi: 10.1016/j.hal.2016.01.008

Haller, G., Hadjighasem, A., Farazmand, M., & Huhn, F. (2016). Defining coherent vortices objectively from the vorticity. *J. Fluid Mech*, *795*, 1136–173.

Haller, G., & Poje, A. (1998). Finite time transport in aperiodic flows. *Physica D*, *119*, 352–380.

Haza, A., Özgökmen, T., & Hogan, P. (2016). Impact of submesoscales on surface material distribution in a Gulf of Mexico mesoscale eddy. *Ocean Modelling*, *107*, 28 - 47. Retrieved from `http://www.sciencedirect.com/science/article/pii/S1463500316301135` doi: http://dx.doi.org/10.1016/j.ocemod.2016.10.002

Hernández-Carrasco, I., Alou-Font, E., Dumont, P.-A., Cabornero, A., Allen, J., & Orfila, A. (2020). Lagrangian flow effects on phytoplankton abundance and composition along filament-like structures. *Progress in Oceanography*, *189*, 102469. doi: https://doi.org/10.1016/j.pocean.2020.102469

Hernández-Carrasco, I., López, C., Hernández-García, E., & Turiel, A. (2011). How reliable are finite-size Lyapunov exponents for the assessment of ocean dynamics? *Ocean Modelling*, *36*(3-4), 208 - 218. doi: 10.1016/j.ocemod.2010.12.006

Klein, P., & Lapeyre, G. (2009). The oceanic vertical pump induced by mesoscale and submesoscale turbulence. *Annu. Rev. Mar. Sci.*, *1*, 351–375.

Klein, P., Lapeyre, G., Siegelman, L., Qiu, B., Fu, L.-L., Torres, H., ... Le Gentil, S.

(2019). Ocean-scale interactions from space. *Earth and Space Science*, *6*(5), 795-817. doi: https://doi.org/10.1029/2018EA000492

Lévy, M., Franks, P., & Smith, K. (2018). The role of submesoscale currents in structuring marine ecosystems. *Nat Commun*, *9*, 4758. doi: 10.1038/s41467-018-07059-3

Lévy, M., Jahn, O., Dutkiewicz, S., & Follows, M. J. (2014). Phytoplankton diversity and community structure affected by oceanic dispersal and mesoscale turbulence. *Limnology and Oceanography: Fluids and Environments*, *4*(1), 67-84. doi: 10.1215/21573689-2768549

Malviya, S., Scalco, E., Audic, S., Vincent, F., Veluchamy, A., Poulain, J., ... Bowler, C. (2016). Insights into global diatom distribution and diversity in the world's ocean. *Proceedings of the National Academy of Sciences*, *113*(11), E1516–E1525. doi: 10.1073/pnas.1509523113

McGillicuddy, D., Robinson, A., Siegel, D., Jannasch, H., Johnson, R., Dickey, T., ... Knap, A. (1998). Influence of mesoscale eddies on new production in the Sargasso Sea. *Nature*, *394*, 263–265.

McGillicuddy, D. J. (2016). Mechanisms of physical-biological-biogeochemical interaction at the oceanic mesoscale. *Annual Review of Marine Science*, *8*(1), 125-159. doi: 10.1146/annurev-marine-010814-015606

Mezić, I., Loire, S., Fonoberov, V. A., & Hogan, P. (2010). A New Mixing Diagnostic and Gulf Oil Spill Movement. *Science*, *330*(6003), 486–489. doi: 10.1126/science.1194607

Morales-Márquez, V., Hernández-Carrasco, I., Fox-Kemper, B., & Orfila, A. (2022). Ageostrophic contribution by the wind and waves induced flow to the lateral stirring in the mediterranean sea in the Mediterranean Sea. *under revision in Journal of Geophysical Research: Oceans*. doi: https://doi.org/10.31223/X56D25

Morrow, R., Fu, L.-L., Ardhuin, F., Benkiran, M., Chapron, B., Cosme, E., ... Zaron, E. D. (2019). Global Observations of Fine-Scale Ocean Surface Topography With the Surface Water and Ocean Topography (SWOT) Mission. *Frontiers in Marine Science*, *6*. doi: 10.3389/fmars.2019.00232

Navarro, G., Almaraz, P., Caballero, I., Vazquez, A., & Huertas, I. E. (2017). Reproduction of spatio-temporal patterns of major mediterranean phytoplankton groups from remote sensing oc-cci data. *Frontiers in Marine Science*, *4*, 246. doi: 10.3389/fmars.2017.00246

Navarro, G., Alvain, S., Vantrepotte, V., & Huertas, I. (2014). Identification of dominant phytoplankton functional types in the mediterranean sea based on a regionalized remote sensing approach. *Remote Sensing of Environment*, *152*, 557 - 575. doi: https://doi.org/10.1016/j.rse.2014.06.029

Rynearson, T., Richardson, K., Lampitt, R., Sieracki, M., Poulton, A., Lyngsgaard, M., & Perry, M. (2013). Major contribution of diatom resting spores to vertical flux in the sub-polar North Atlantic. *Deep Sea Research Part I: Oceanographic Research Papers*, *82*, 60-71. doi: https://doi.org/10.1016/j.dsr.2013.07.013

Storm, T., Boettcher, M., Grant, M., Zuhlke, M., Fomferra, N., Jackson, T., & et al. (2013). Product User Guide, Ocean Colour Climate Change Initiative.

Tréguer, P., Bowler, C., Moriceau, B., & et al. (2018). Influence of diatom diversity on the ocean biological carbon pump. *Nature Geosci.*, *11*, 27–37. doi: 10.1038/s41561-017-0028-x

Wilkins, D., van Sebille, E., Rintoul, S. R., Lauro, F. M., & Cavicchioli, R. (2013). Advection shapes southern ocean microbial assemblages independent of distance and environment effects. *Nature Communications*, *4*(2457). doi: 10.1038/ncomms3457

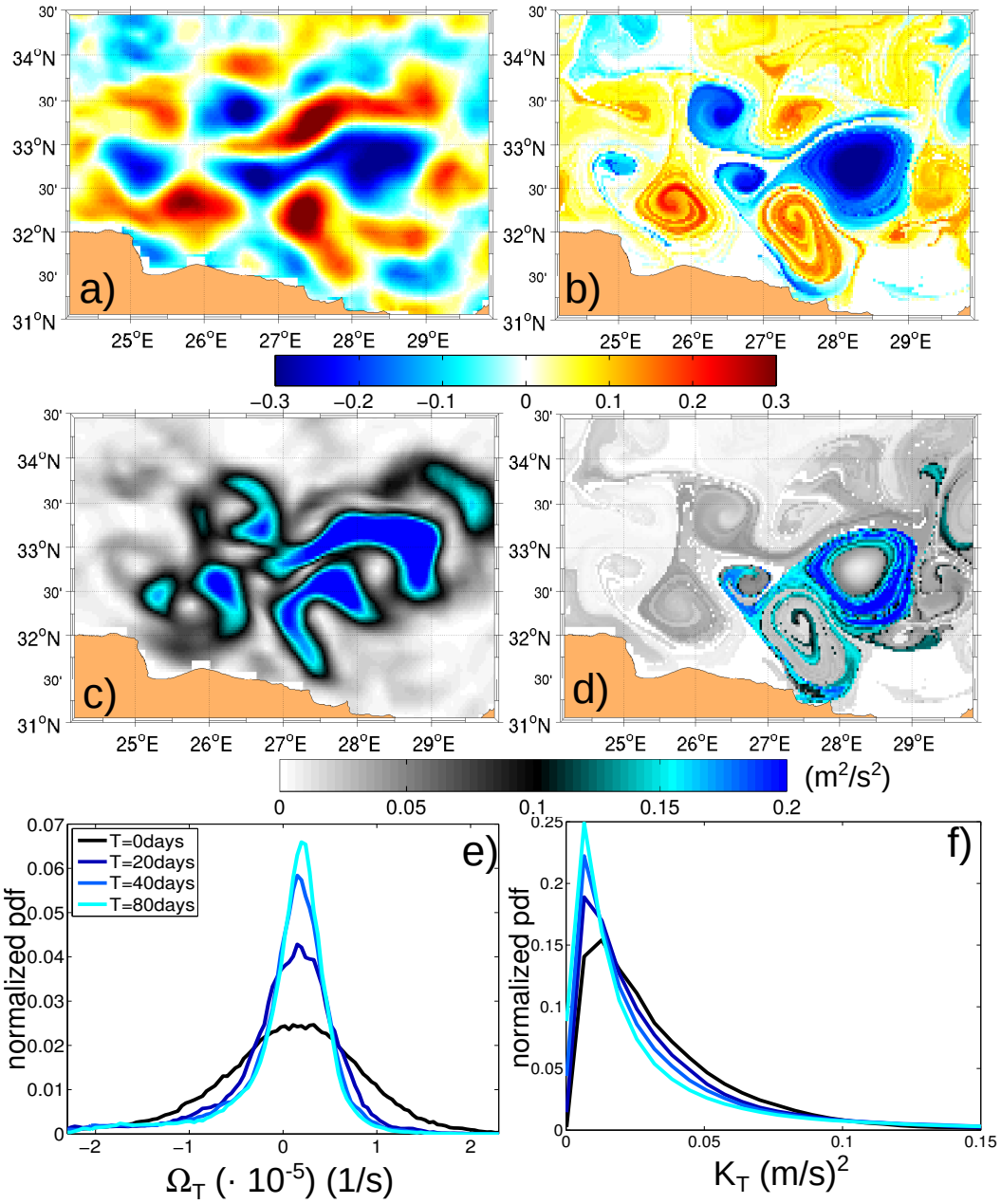

Figure 1. (A) and (B) show snapshots corresponding to March 22, 2016 of Ω_0 and Ω_{40} divided by Coriolis parameter. (C) and (D) show K_0 and K_{40} for the same date. Panels (E) and (F) show the PDF for Ω_T and K_T, respectively, using values from weekly snapshots over 2006-2016 for different integration times, T.

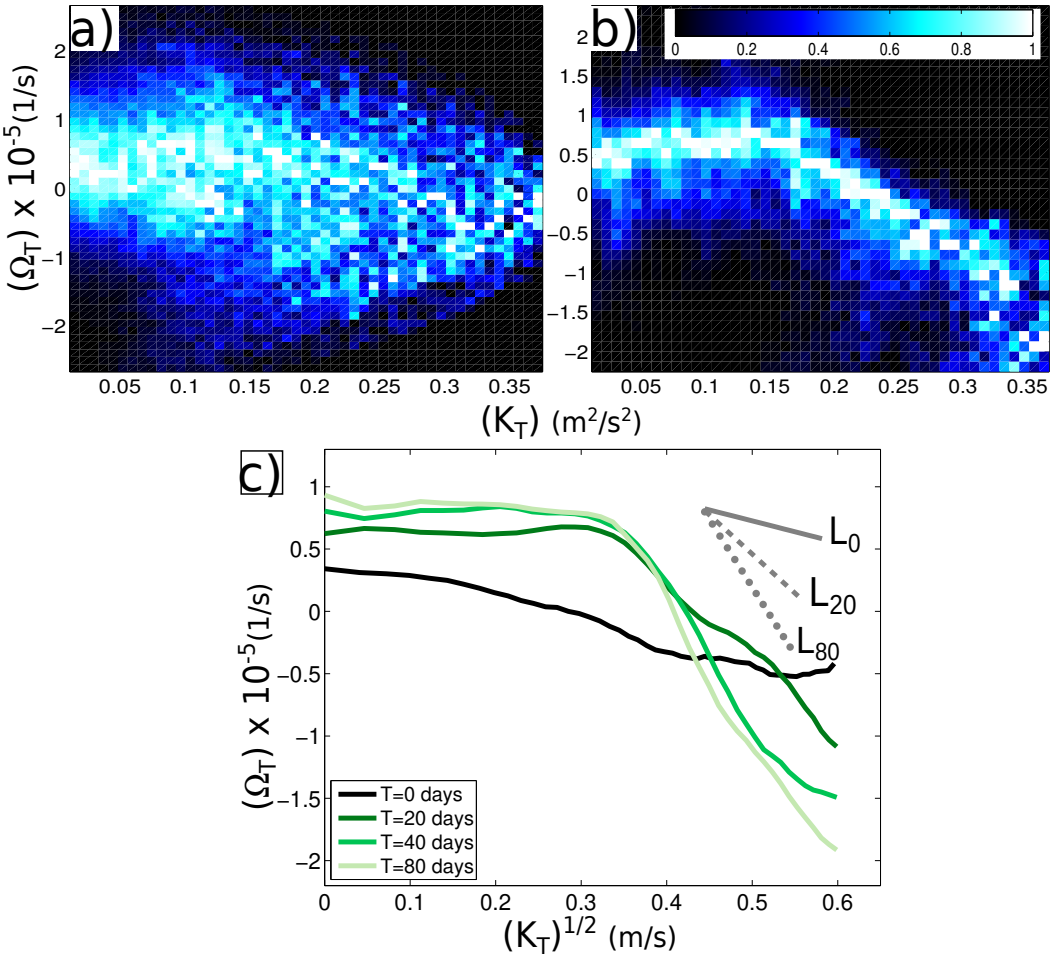

Figure 2. Probability distributions of Ω_T conditioned by K_T for two different time periods of integration, T = 0 days (panel *A*) and T = 40 days (panel *B*). The brightest color (light blue) corresponds to the maximum probability at each column; the darkest color (pure black) corresponds to zero. (*C*) shows functional dependence between Ω_T *vs* $K_T^{1/2}$ for different integration times T. Correlation coefficient are computed from co-variance dependence, obtaining R^2=0.19 for T=0 days; R^2=0.52 for T=20 ; R^2=0.69 for T =40 and R^2 =0.76 for T=80 days. Slopes resulting from the linear regression fit analysis of the functional dependencies between Ω_T *vs* $K_T^{1/2}$ for T= 0 , 20 and 80 days are shown as grey lines in *C*. Their corresponding length scales are L_0= 56 km L_{20} = 29 km and L_{80} =15 km.

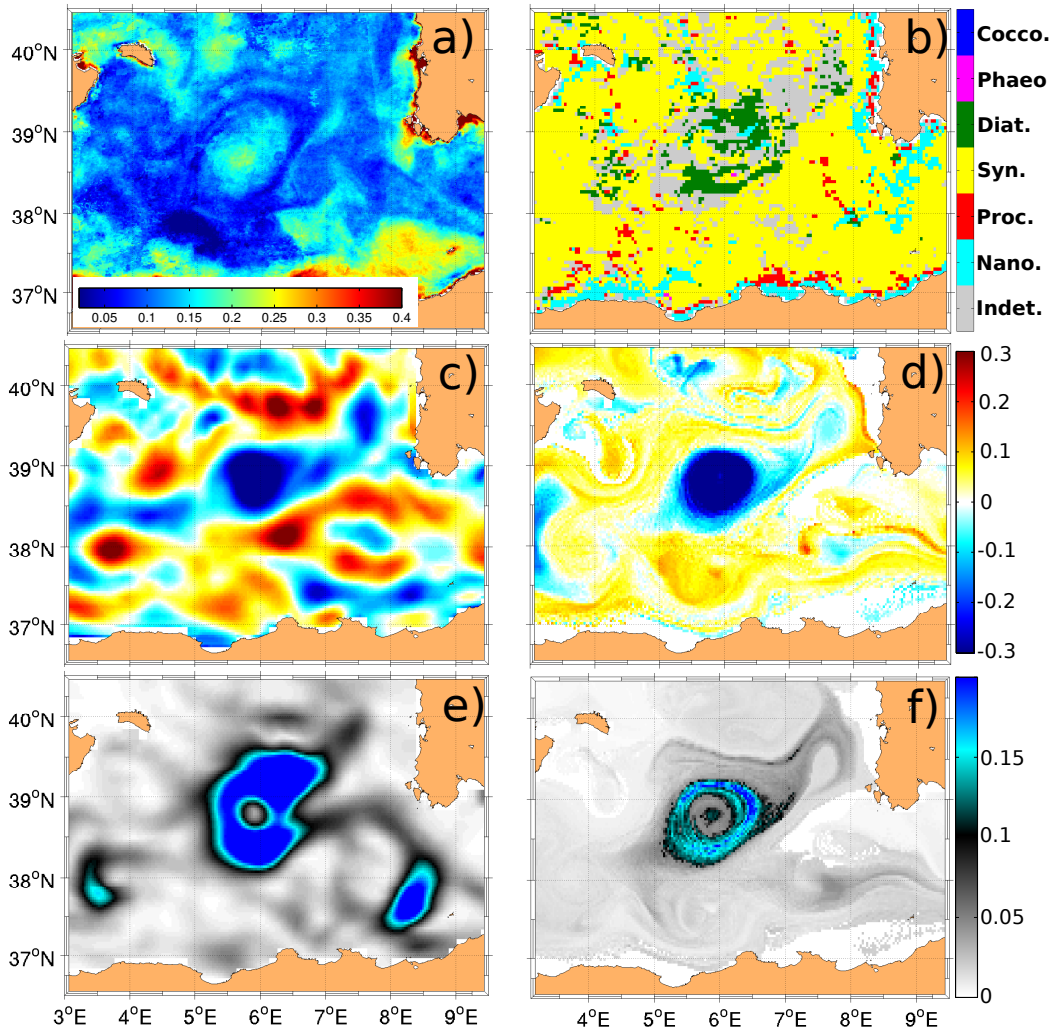

Figure 3. (A) Chlorophyll (a) (in mg/m^3) derived from Ocean color satellite data; (B) map of dominant phytoplankton functional types retrieved from the PHYSAT-Med product corresponding to the period: May 28, 2009 - June 07, 2009; (C) and (E) are the Eurelian vorticity, Ω_0, divided by Coriolis, and Eulerian EKE, K_0 (in m^2/s^2), both averaged over 10 daily snapshots (May 28, 2009 - June 07, 2009); (D) and (F)) are the Lagrangian vorticity, Ω_{40}, and Lagrangian EKE, K_{40} (in m^2/s^2), for T=40 days, and averaged over the same period.

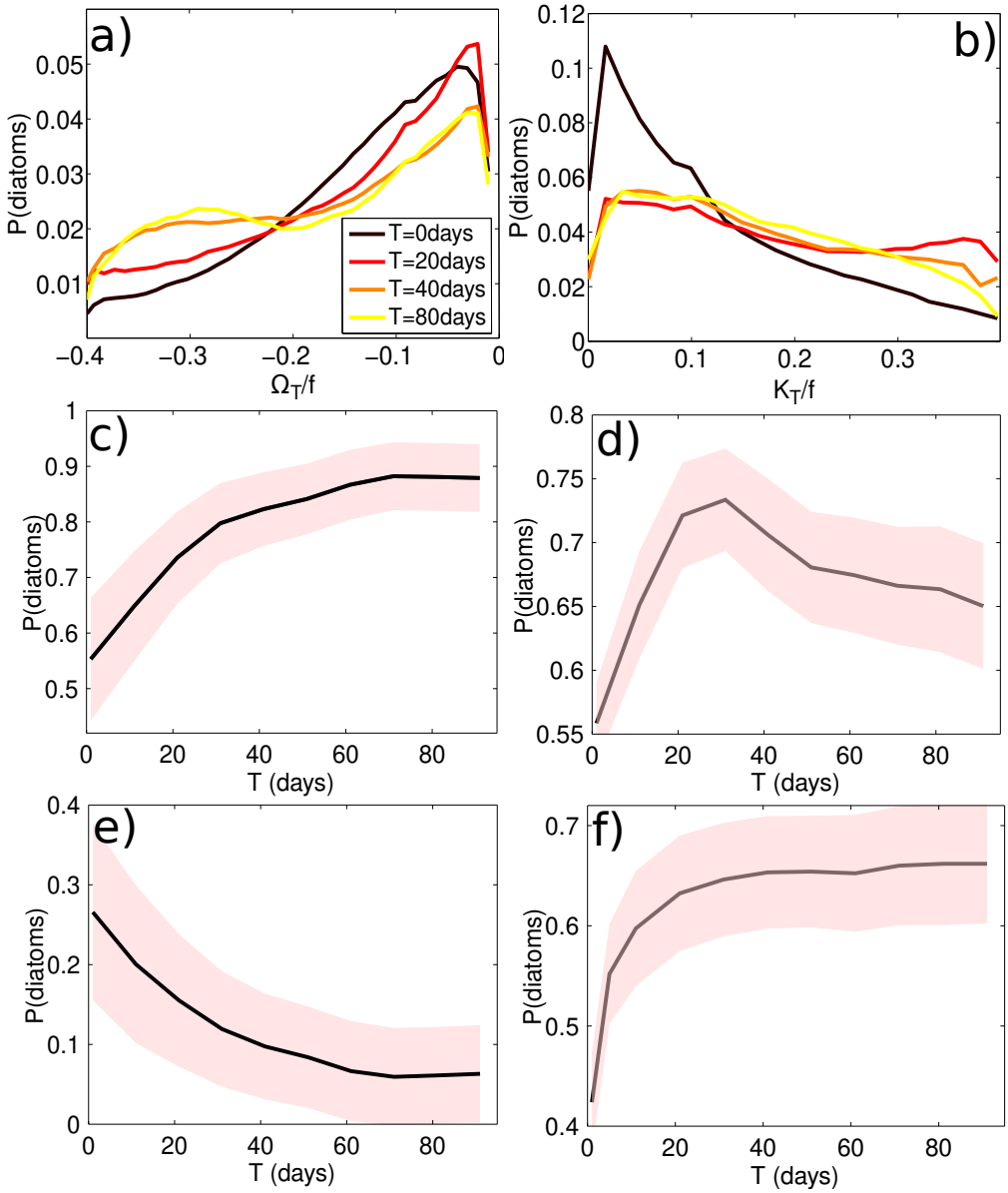

Figure 4. Probability density function of the normalized number of diatoms, or diatoms abundance, (to unity area) versus values of Ω_T (A) and K_T (B). Normalized diatom abundance as a function of the time integration T found in regions of high negative (C), positive Ω_T (E) and high K_T (D); and in regions high negative Ω_T and high K_T simultaneously (F).